South American monsoon response to iceberg discharge in the North Atlantic

Nicolás M. Stríkis[a,b,1], Francisco W. Cruz[b], Eline A. S. Barreto[b], Filipa Naughton[c,d], Mathias Vuille[e], Hai Cheng[f,g], Antje H. L. Voelker[c,d], Haiwei Zhang[g], Ivo Karmann[b], R. Lawrence Edwards[f], Augusto S. Auler[h], Roberto Ventura Santos[i], and Hamilton Reis Sales[j]

[a]Departamento de Geoquímica, Universidade Federal Fluminense, 24020-141 Niterói, Brazil; [b]Instituto de Geociências, Universidade de São Paulo, 05508-080 São Paulo, Brazil; [c]Instituto Português do Mar e da Atmosfera, 1495-006 Lisboa, Portugal; [d]Center of Marine Sciences, Algarve University, 8005-139 Faro, Portugal; [e]Department of Atmospheric and Environmental Sciences, University at Albany, State University of New York, Albany, NY 12222; [f]Department of Earth Sciences, University of Minnesota, Minneapolis, MN 55455; [g]Institute of Global Environmental Change, Xi'an Jiaotong University, 710049, Shaanxi, China; [h]Instituto do Carste, 30360-260 Belo Horizonte, MG, Brazil; [i]Instituto de Geociências, Universidade de Brasília, 70297-400 Brasília, Brazil; and [j]Instituto Federal de Educação, Ciência e Tecnologia do Norte de Minas Gerais, 39480-000 Januária, Brazil

Edited by Wallace S. Broecker, Columbia University, Palisades, NY, and approved February 12, 2018 (received for review October 10, 2017)

Heinrich Stadials significantly affected tropical precipitation through changes in the interhemispheric temperature gradient as a result of abrupt cooling in the North Atlantic. Here, we focus on changes in South American monsoon precipitation during Heinrich Stadials using a suite of speleothem records covering the last 85 ky B.P. from eastern South America. We document the response of South American monsoon precipitation to episodes of extensive iceberg discharge, which is distinct from the response to the cooling episodes that precede the main phase of ice-rafted detritus deposition. Our results demonstrate that iceberg discharge in the western subtropical North Atlantic led to an abrupt increase in monsoon precipitation over eastern South America. Our findings of an enhanced Southern Hemisphere monsoon, coeval with the iceberg discharge into the North Atlantic, are consistent with the observed abrupt increase in atmospheric methane concentrations during Heinrich Stadials.

Heinrich Stadial | South American monsoon | speleothem | ice-rafted detritus

The last Glacial Period, characterized by abrupt transitions between extreme cold (Greenland Stadials, GS) and mild (Greenland Interstadials, GI) climate states, provides evidence of rapid coupled ocean–atmosphere reorganizations at millennial timescale (e.g., refs. 1–4). At least 6 out of the 26 well-recognized GS events are marked by episodes of massive ice-rafted detritus (IRD) deposition (5–7), which were preceded by extreme cooling events in the North Atlantic and are associated with the so-called Heinrich Stadials (HS) (e.g., refs. 3, 8, and 9).

This millennial-scale climate variability recorded in mid- and high latitudes of the North Atlantic was transmitted to the tropics through changes in the intensity of the NE trade winds and cross-equatorial temperature gradients that drive the mean position of the Intertropical Convergence Zone (ITCZ) (10–13). During HS events, the preferential cooling of the Northern Hemisphere led to a southward displacement of the ITCZ, whose strength and position are closely tied to the interhemispheric surface-air temperature and sea-surface temperature (SST) gradient (11, 12, 14). Over the North Atlantic, the connection between high latitude and tropical surface cooling occurs through equatorward advection of cold air masses to midlatitudes in the area of the North Atlantic's subtropical High/Azores High (10).

Climatic expression of such millennial cold events is even more pronounced in midlatitudes as evidenced by sharp declines of Pine forests in southwestern Europe (15) (reflecting extreme cold atmospheric conditions) that precede episodes of iceberg surge. These complex events are synchronous with the two distinct phases of HS in the northern North Atlantic (16). However, there is no understanding so far of how the southward displacement of the thermal front as far south as 35–37° N (15, 17, 18) affected the interplay between SST and atmospheric circulation at subtropical and tropical latitudes during the two phases of an HS, that is, the cold phase preceding maximum IRD deposition and the IRD peak itself.

Similarly, an abrupt weakening of the East Asian monsoon (19) and a strengthening of the monsoon in eastern South America is recorded during HS1 at the time of IRD deposition (20–23). Furthermore, peaks in the global atmospheric methane concentration associated with tropical wetland expansion appear to be synchronous with episodes of iceberg discharge in the North Atlantic (24). Nevertheless, despite the dominant influence of HS on the tropical hydrologic cycle, most of our current understanding of how HS affected the global monsoon stems from remote marine and ice core records, rather than in situ archives directly recording changes in tropical precipitation.

Here we explore the timing and magnitude of changes in South American Monsoon precipitation during HS based on in situ speleothem records to assess its sensitivity to changes in coupled ocean–atmosphere interactions, propagating from the Northern Hemisphere high latitudes to tropical regions.

Significance

Here, we present a precisely dated speleothem record of South American monsoon precipitation covering the period encompassed by the last six Heinrich Stadials. Our monsoon record allows us to determine the timing of regional hydroclimatic expression of Heinrich Stadials over tropical lowland South America. By comparing our record with sea-surface temperature reconstructions from the subtropical North Atlantic, our results provide evidence connecting South American monsoon precipitation and methane release with the events of iceberg discharge depicted by the deposits of ice-rafted detritus. These results are relevant to climate modelers and paleoclimatologists interested in abrupt climate change, tropical–extratropical climate teleconnections, and paleo-reconstructions of the monsoon and the tropical hydrologic cycle.

Author contributions: N.M.S., F.W.C., I.K., A.S.A., R.V.S., and H.R.S. performed research; N.M.S., E.A.S.B., H.C., H.Z., and R.L.E. analyzed data; and N.M.S., F.W.C., F.N., M.V., and A.H.L.V. wrote the paper.

The authors declare no conflict of interest.

This article is a PNAS Direct Submission.

Data deposition: The sequences reported in this paper have been deposited in the NOAA Paleoclimatology Database, https://www.ncdc.noaa.gov/paleo/study/23510.

[1]To whom correspondence should be addressed. Email: strikis@gmail.com.

This article contains supporting information online at www.pnas.org/lookup/suppl/doi:10.1073/pnas.1717784115/-/DCSupplemental.

Published online March 26, 2018.

Site Descriptions

Monsoon precipitation over eastern South America is reconstructed from isotopic records derived from speleothems, sampled in multiple caves located in Central-Eastern and Northeastern Brazil. The record from Central-Eastern Brazil is composed of a suite of nine stalagmites sampled in two caves: Lapa Grande (LG) (14°22′S, 44°17′W) and Lapa Sem Fim (LSF) (16°09′S, 44°36′W). The distance between the two caves is about 190 km (Fig. S1). The record from Northeast Brazil is composed of two stalagmites sampled in two caves located 1 km apart from one another: Paixão (PX) (12°37′S, 41°01′W) and Marota (MAG) (12°35′S, 41°02′W). At all cave sites the precipitation occurs almost exclusively during the active period of the South American Monsoon System (SAMS), between October and April, with a maximum activity between November and February when almost 70% of the total annual precipitation occurs (*Precipitation at the Study Site* and Fig. S2).

The isotopic composition of rainfall at the sites during the monsoon season is primarily influenced by the amount of rainfall and is characterized by a decrease in $\delta^{18}O$ with increasing rainfall totals on seasonal and interannual timescales (Figs. S3), although the degree of rainfall upstream might have a significant influence on $\delta^{18}O$ (25, 26). In fact, $\delta^{18}O$ at the nearest station maintained by the International Atomic Energy Agency (IAEA) Global Network of Isotopes in Precipitation (GNIP), Brasilia, is not only closely anticorrelated

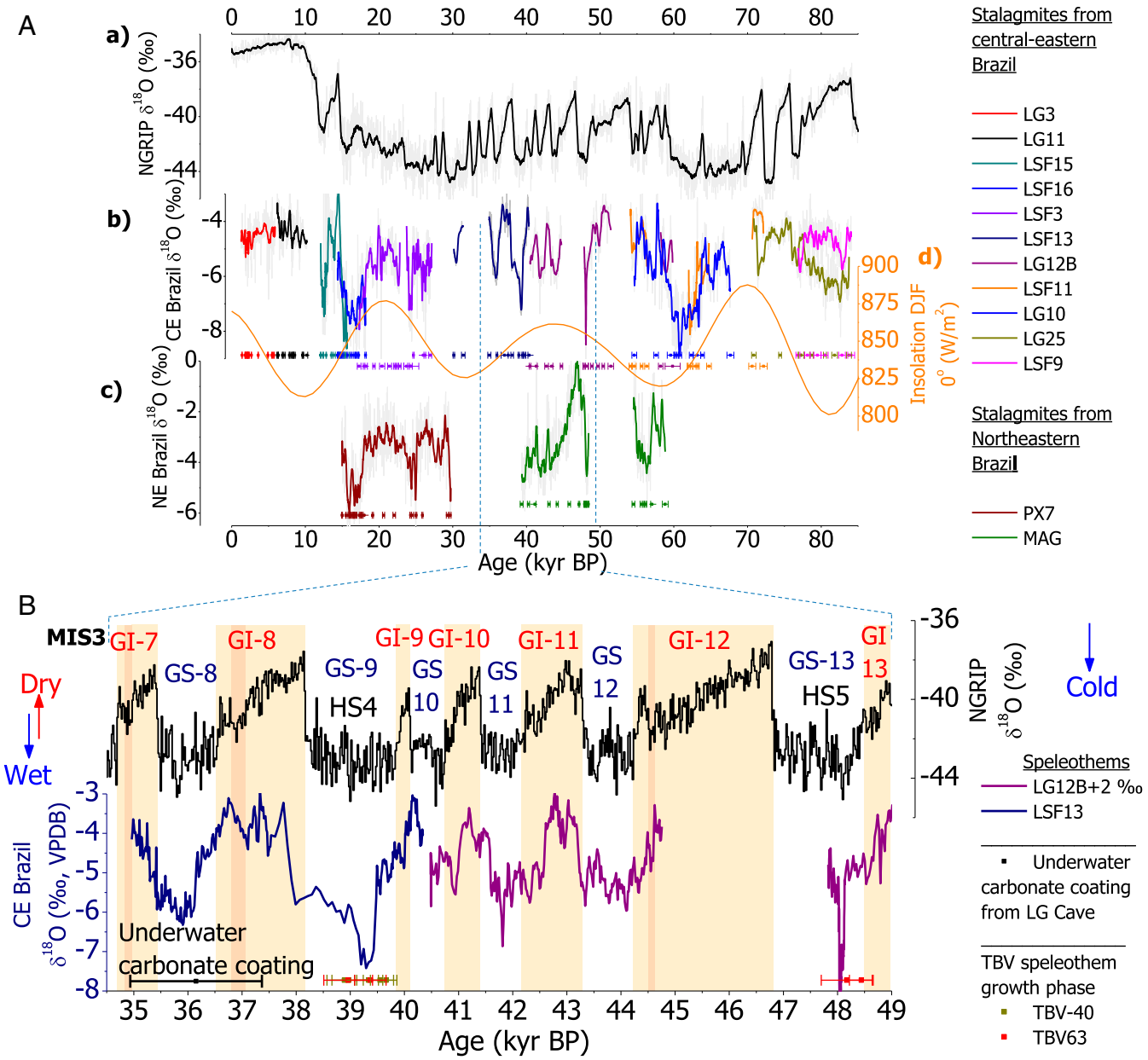

Fig. 1. Comparison between eastern South American monsoon precipitation and Greenland ice core. (*Top*) (*A*, *a*) Two-hundred-year running mean North Greenland Ice Core Project (NGRIP) ice core $\delta^{18}O$ record on the annual-layer-counted GICC05 (3) (200-y running mean, black line). (*A*, *b* and *c*) $\delta^{18}O$ speleothem record from Central-Eastern (CE) and Northeastern (NE) Brazil [this study and Strikis et al. (23)] (200-y running mean, thick lines). (*A*, *d*) Austral summer insolation curve (December, January, February) calculated for 0° latitude (52) (orange). (*B*) Detail of millennial-scale variability in Greenland ice core $\delta^{18}O$ record and Central-Eastern Brazil speleothem $\delta^{18}O$ record. Colored error bars represent age uncertainties of ^{230}Th dates of the corresponding speleothem used in this study and the speleothem growth phases from Toca da Boa Vista cave (TBV) from Wang et al. (28). Red and dark-blue numbers define the GI and GS events, respectively, according to Rasmussen et al. (3).

with local precipitation, but a faithful recorder of regional precipitation over the eastern South American domain (Fig. S3).

Results and Discussion

The speleothem-derived stable oxygen isotope ($\delta^{18}O$) records presented here are based on more than six thousand measurements for $\delta^{18}O$, yielding a mean temporal resolution of ~20 y (Fig. 1). The chronological control of these speleothem records is based on 128 new ^{230}Th dates covering the last 84 ky (Dataset S1). For the time period from 14.37 to 19.30 ky B.P. we present the combined speleothem record from Stríkis et al. (23), which is based on three stalagmite records: LSF16, LSF3, and PX7. In addition, here we use an updated age model of PX7 stalagmite, which includes four additional ages between 15.51 and 17.37 ky B.P. We also extended the isotope record of LSF3 (17.3–19.30 ky B.P.) to 26.95 ky B.P. (Dataset S1). Although the $\delta^{18}O$ values from the LG speleothem record are ~1.5‰ more enriched than those from LSF, both isotope records describe consistent variations of similar amplitude on orbital to millennial timescales (Fig. 1). In particular, the isotope record is characterized by numerous millennial-scale events of high amplitude, recording abrupt isotopic excursions of about 3‰ with an average duration of less than 100 y. Here we demonstrate that these abrupt events of increased SAMS activity during the HS are coeval, within dating uncertainties, with the periods of IRD deposition in the eastern subtropical North Atlantic (Fig. 2).

There is no clear relationship between monsoon precipitation over Central-Eastern Brazil and changes in summer insolation over the last 85 ky, although some coupling appears to occur between about 80 and 60 ky B.P., also observed in $\delta^{18}O$ speleothem records from the western Amazon basin (27) (Fig. 1).

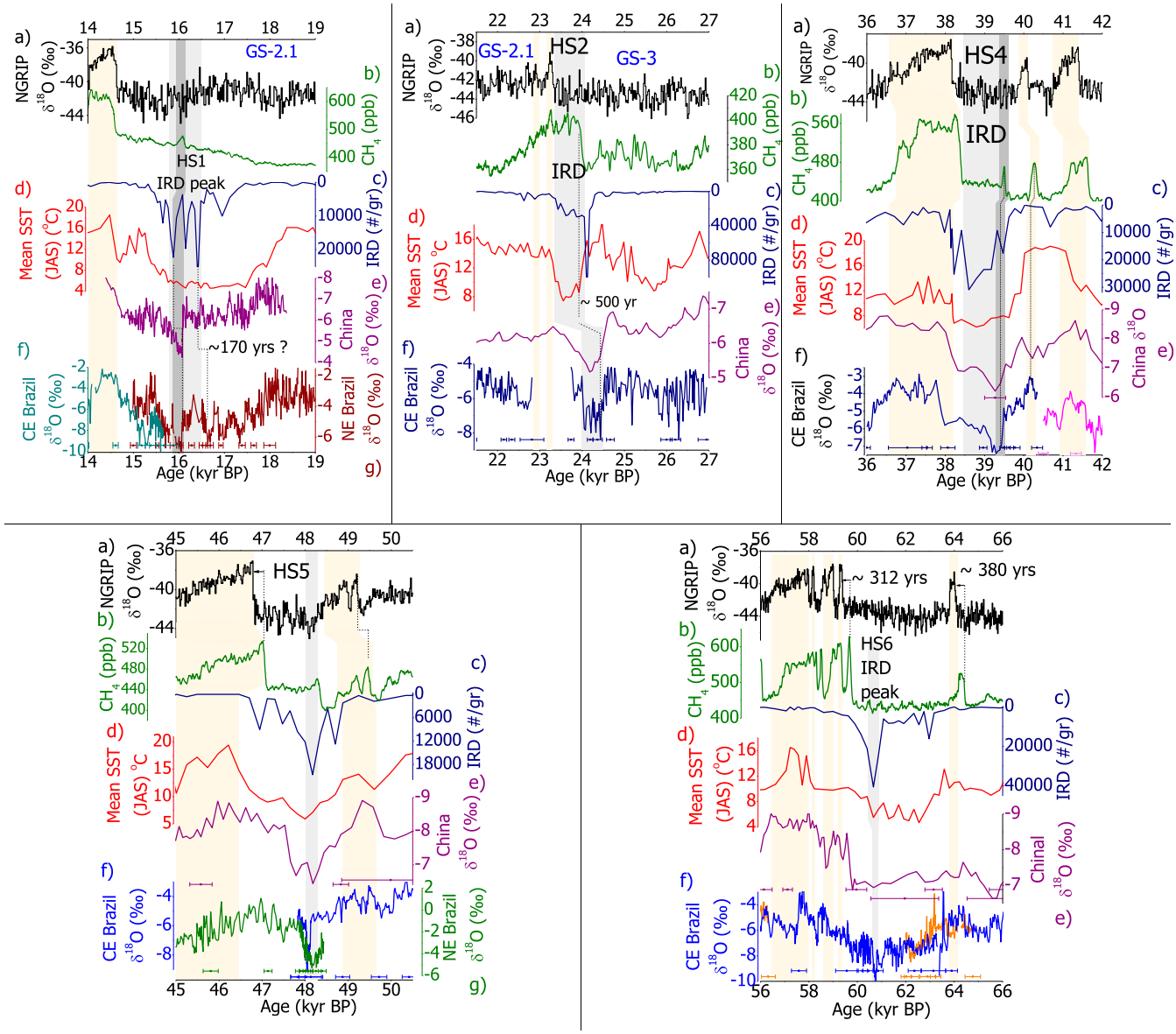

Fig. 2. Comparison between IRD, atmospheric CH_4, North Atlantic SST, and monsoon precipitation. (*A*) NGRIP ice core $\delta^{18}O$ record on the annual-layer-counted GICC05 (3). (*B*) Atmospheric methane concentration from West Antarctic ice sheet divide core in the WD2014 timescale (24). (*C*) IRD > 150 μm from Iberian Margin (core MD95-2040) (15). (*D*) Summer SST reconstruction from Iberian Margin based on planktonic foraminiferal census count (core MD95-2040) (18, 35). The time series of MD95-2040 was synchronized with Greenland climate records using the GICC05 timescale. (*E*) Eastern Asia monsoon record from Hulu Cave (18, 37). (*F* and *G*) Paleo monsoon reconstruction from Central-Eastern (CE) and Northeastern (NE) Brazil based on $\delta^{18}O$ isotope profile from speleothems [this study and Stríkis et al. (23)]. Gray bars delimit the timing of main phase of IRD deposition during HS.

On the other hand, precipitation over eastern South America was strongly modulated by millennial-scale events during the last Glacial Period, leading to synchronous climate variations over the South American tropics and high-latitude areas of the Northern Hemisphere (Figs. 1 and 2). During Marine Isotope Stage (MIS) 3 (~27–60 ky BP) in particular, variations in the intensity of monsoon precipitation respond in phase to the abrupt temperature oscillations of the GS and GI cycles recorded in the $\delta^{18}O$ isotope curve of Greenland ice cores (3, 9) (Fig. 1*B*). The impact of GS phases on the hydrologic regime over eastern tropical South America is also documented by past water-table fluctuations recorded in calcite rimes at the LG cave walls. A subaqueous carbonate coating, located along the edge of the cave walls on a currently dry conduit, is ^{230}Th dated at 35.87 ± 1.2 ky B.P., pointing to significantly increased groundwater recharge during GS-8 (36.58–35.48 ky B.P.) (Fig. 1*B* and Fig. S4). This scenario is also consistent with the episodic speleothem growth and tufa formation recorded during GS and HS in the current semiarid areas of Northeast Brazil (28).

While the response of the SAMS to GS and GI phases documented in our speleothem record is consistent with the response reported in previous studies (14, 22, 29–31), this is, to our knowledge, the first observational evidence directly relating the SAMS response to Northern Hemisphere sea ice expansion and episodes of iceberg discharge and IRD deposition, as for example recorded in midlatitudes of the North Atlantic, off the Iberian Peninsula (9, 15, 17). While evidence for the occurrence of episodic wet events in the current semiarid areas of Northeastern Brazil during HS is well established (14, 21, 22), our higher-resolution and more precisely dated speleothem records allow distinguishing between the general strengthening of the South American monsoon in response to North Atlantic cooling and the additional monsoon enhancement during the maximum IRD deposition, thereby connecting the iceberg discharge with reorganization of tropical monsoon circulation.

Direct comparisons between continental and marine paleoclimate archives extending to the Glacial Period can be challenging since imprecision in the marine core chronology linked to ocean ^{14}C reservoir age uncertainties makes it difficult to establish a precise chronology for the timing of environmental and climate changes (32). Furthermore, a Heinrich event may be time-transgressive, which renders the chronology of the Heinrich layer/event even more challenging (3, 33). On the other hand, the tuning of the $\delta^{18}O$ record of planktonic foraminifera with the millennial-scale GS/GI oscillations in the Greenland $\delta^{18}O$ record may circumvent part of this problem, allowing establishment of a better comparison between monsoon variability in South America and high- and midlatitude SST variations in the North Atlantic. This approach facilitates the assessment of the imprint of HS on the South American monsoon. To allow for a direct comparison with the eastern South America speleothem records, the Greenland Ice Sheet Project 2 (GISP2)-related chronology of deep-sea core MD95-2040 (34, 35) was transferred to the annual-layer-counted Greenland ice core chronology 2005 (GICC05) (3) following the GI/GS boundary identifications (presented in Fig. 2).

The coupling between eastern North Atlantic SST and the SAMS is evident during HS1, HS2, HS5, and HS6, when a substantial depletion in the speleothem $\delta^{18}O$ occurs independently of changes in temperature over high-latitude areas (Fig. 2). During HS1 a negative excursion recorded in the speleothem isotopic composition that begins in the middle of GS2.1 at 18 ky B.P. coincides with the cooling in the eastern subtropical North Atlantic. However, a more pronounced drop in the speleothem $\delta^{18}O$ record occurs at 16.1 ky B.P., contemporaneous with a major peak in IRD deposition, identified in marine records from the subtropical North Atlantic (e.g., refs. 23 and 36–38) (Fig. 3). Also, Stern and Lisiecki (38) recognize a rapid decrease in the ^{14}C reservoir age along with the 16 ky B.P. IRD peak, indicating a strong stratification of the upper water column associated with the massive freshwater release during the main phase of IRD deposition.

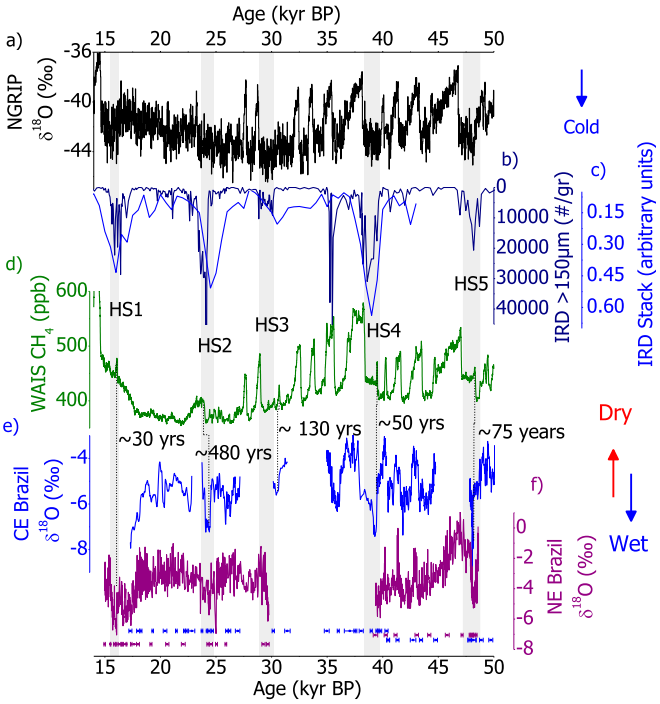

Fig. 3. Comparison between high-latitude North Atlantic surface temperature, IRD, atmospheric CH_4, and monsoon precipitation. (*A*) NGRIP ice core $\delta^{18}O$ record on the annual-layer-counted GICC05 (3). (*B*) IRD from Iberian Margin (core MD95-2040) (18, 35). (*C*) IRD stack of North Atlantic sediment cores (38). (*D*) Atmospheric methane concentration from West Antarctic ice sheet divide core in the WD2014 timescale (24). (*E* and *F*) Paleo monsoon reconstruction from CE and NE Brazil based on $\delta^{18}O$ isotope profile from speleothems [this study and Stríkis et al. (23)].

During HS2, the Greenland ice core $\delta^{18}O$ record shows no significant perturbation. On the other hand, speleothem records from central South America [this study and Novello et al. (39)] and the Peruvian Andes (30), as well as SST in core MD95-2040 (18, 35), show significant climate anomalies consistent with the timing of IRD deposition. The abrupt strengthening in the SAMS from 24.6 to 24.0 ky B.P. also coincides with a period of SST cooling at the time of HS2 IRD deposition (Fig. 2 and Fig. S5). However, unlike HS1, during HS2 monsoon precipitation in eastern South America, SST anomalies in the eastern subtropical North Atlantic and IRD deposition are synchronous, taking place at the same time. During the HS1, on the other hand, the IRD maximum occurs nearly 1,000 y after the monsoon strengthening and the surface ocean cooling in the North Atlantic.

Similar connections between IRD deposition and SAMS intensification are also evident during HS4, HS5, and HS6, when a strengthening of the SAMS over eastern South America again coincides with episodes of IRD deposition as evidenced by the sudden and large $\delta^{18}O$ decrease (sometimes >3‰ in magnitude) at the time of Heinrich-layer deposition in the eastern subtropical North Atlantic (Figs. 2 and 3). However, the relationship between SAMS activity and iceberg surge is not linear. During HS4, monsoon precipitation is intensified with the onset of IRD deposition and not necessarily during its peak phase (Figs. 2 and 3). Notably, no equivalent anomalies are recorded in the $\delta^{18}O$ of the Greenland ice cores. The maximum $\delta^{18}O$ drop in speleothem LSF13 and LG12B during HS4 and HS5 are contemporaneous with the episodic event of speleothem growth (TBV-40 and 63) observed in semiarid Northeastern Brazil (28), respectively (Fig. 1). During HS4 and HS5 in particular, a positive excursion toward dry conditions occurs over the central Peruvian Andes with no counterpart in

the speleothem $\delta^{18}O$ record from eastern South America and the western Amazon basin (31) (Fig. S6). The dry excursion along the western border of the SAMS domain indicates that HS may at times affect monsoon rainfall differently along the eastern and western fringe of the SAMS region. Antarctic forcing may also play a significant role during some of these abrupt events as previously suggested by Kanner et al. (30) (Fig. S6).

The abrupt strengthening recorded in the SAMS during HS1, HS2, HS4, and HS5 also coincides with abrupt increases in the atmospheric methane concentration (24) (Fig. 2). During HS1 the $\delta^{18}O$ minimum at 16.1 ky B.P. identified in the speleothem records from Central-Eastern and Northeastern Brazil coincides with a spike in atmospheric methane at 16.13 ky B.P. Similarly, during HS2 and HS5 sudden enhancements of monsoon precipitation over eastern South America coincide with abrupt increases in the global methane concentration (24) (Fig. 2). Neither record has a similar abrupt counterpart in the surface temperature record at high northern latitudes, strengthening the argument that much cooler temperatures related to the peak of IRD deposition during the HS events affected tropical precipitation, leading to an increase in global atmospheric methane as a consequence of a substantial enhancement of monsoon precipitation over tropical land areas of the Southern Hemisphere (24).

The close coupling between monsoon precipitation over eastern South America and Northern Hemisphere midlatitude temperature can be explained by the latitudinal shift in the mean position of the ITCZ as a consequence of changes in the tropical interhemispheric SST gradient (12, 40). The surface cooling in the subtropical North Atlantic is likely caused by the strengthening of the Azores High during GS and HS, thereby changing the interhemispheric SST gradient and displacing the ITCZ southward (15). In this scenario, fresh water release associated with the melting iceberg and consequent IRD deposition led to the expansion of sea-ice cover, displacing the oceanic thermal front southward hence, affecting global monsoon precipitation. This concept is reinforced by the striking antiphasing between millennial-scale events in speleothem isotope records from the South American monsoon domain (29–31) and Northern Hemisphere monsoon precipitation record (41). During HS the annually resolved terrigenous input from the Cariaco Basin (41) points to severe drought concordant with midlatitude SST reconstructions from the eastern North Atlantic (Fig. S7). In the same way, dry conditions over the eastern Asian Monsoon (42) domain coincide with periods of maximum monsoon precipitation over central South America (Fig. 2). A maximum sea-ice extent during the HS (43) may have resulted in a southward shift of the sub-Arctic front affecting surface temperature at mid- and low latitudes and forcing a southward displacement of the ITCZ. In fact, for some HS events, as observed during HS2, HS4, and HS5, peaks of strengthening of the polar vortex (calcium ion concentration from ice cores) line up with events of SAMS strengthening (Fig. S7). This would explain the response of SAMS precipitation over eastern South America and the abrupt methane increase at times of IRD deposition in the Iberian Margin (Fig. 3).

Conclusions

Our results suggest that the advection of cold air masses associated with the abrupt reduction of surface temperature in response to massive iceberg surges during the main phase of IRD deposition may have intensified the North Atlantic subtropical High, thereby increasing the advection of moisture into the South American continent. In southwestern Europe marine records located at the Iberian Margin point to a substantial reduction of river discharge coeval with the peak IRD deposition (15). The relationship established between cold surface-water anomalies in the eastern subtropical North Atlantic, dry conditions in southwestern Europe, and positive SAMS anomalies in eastern South America during periods of IRD deposition is similar to a positive North Atlantic Oscillation mode (15, 44). Our results also highlight important regional differences in the precipitation response to HS in the eastern and western part of the SAMS domain, which warrant further study. A zonal precipitation dipole between eastern and western tropical South America has previously been noted to occur on several timescales and in response to a variety of different forcings (32, 45). Finally, our results also highlight the sensitivity of the SAMS to changes in the interhemispheric temperature gradient, which may have implications for future drought scenarios over eastern South American monsoon domains, given the preferential warming of the Northern Hemisphere under future greenhouse gas forcing (46, 47).

Methods

Stable Isotope Analyses. Oxygen isotope ratios are expressed in δ-notation, the per-mil deviation from the VPDB (Vienna Pee Dee Belemnite) standard. For example, for oxygen, $\delta^{18}O = [((^{18}O/^{16}O)\ \text{sample}/(^{18}O/^{16}O)\text{VPDB}) - 1] \times 1{,}000$. For each measurement, ∼200 μg of powder was drilled from the sample and analyzed with an online, automated, carbonate preparation system linked to a Finnigan Delta Plus Advantage mass spectrometer at the University of São Paulo, Brazil. Reproducibility of standard materials is 0.15‰ for $\delta^{18}O$. The stable isotope data presented in this paper will be made available at the NOAA Paleoclimatology datasets.

Age Model. The ages were obtained by using a multicollector inductively coupled plasma mass spectrometry technique (Thermo-Finnigan NEPTUNE) at the University of Minnesota and the Institute of Global Environmental Change, Xi'an Jiaotong University, Xi'an, China following the procedures described by Cheng et al. (48). Most dates present errors (2σ) <1% (Dataset S1). The samples weighing between 150 and 300 mg were dissolved in HNO_3 and equilibrated with a ^{236}U-^{233}U-^{229}Th spike and then separated and purified using methods described by Cheng et al. (48). Initial ^{230}Th values were corrected with a typical bulk earth ratio, that is, atomic ratio of $^{230}Th/^{232}Th = 4.4 \pm 2.2$. The chronology of the samples is established by linear interpolation between ^{230}Th dates.

Previously published age models for Iberian Margin core MD95-2040 below 290 cm (>17 ka) are based on a correlation to the chronology of the GISP2 ice core during MIS 2–4 (e.g., refs. 34 and 36). The correlation of MD95-2040 was done with the GISP2 20/50-y resolution $\delta^{18}O$ record of Stuiver and Grootes (49), for which no corresponding depth intervals are available. Therefore, the following steps were needed to derive corresponding GICC05 ages:

i) calculating GISP2 depths for the GISP2-derived age control points of MD95-2040 using the GISP2 age-depth data of Grootes et al. (50);
ii) transferring the obtained GISP2 depths to corresponding GICC05 ages (modified to year B.P.) using the GISP2 depth to GICC05 age correlation for $\delta^{18}O$ data published by Seierstad et al. (51).

The age model above 290 cm remained unchanged, that is, based on the calibrated ^{14}C ages.

ACKNOWLEDGMENTS. We thank L. Mancine, O. Antunes, and A. Barros for their support during the stable isotope data acquisition at the University of São Paulo. We are grateful to Instituto Brasileiro do Meio Ambiente/Instituto Chico Mendes de Conservação da Biodiversidade (IBAMA/ICMBio) for permission to collect stalagmite samples. This work was supported by Fundação de Amparo à Pesquisa do Estado de São Paulo (FAPESP) Grants 2012/01187-4 and 2016/00299-4 (to I.K.), PhD Fellowship 2011/12087-4 (to N.M.S.), and FAPESP/NSF Research Program on Biodiversity Characterization, Conservation, Restoration and Sustainable (BIOTA) and Dimensions of Biodiversity Grants 2012/50260-6 and 2013/50297 (to F.W.C.) and NSFC 41731174 (to H.Z.). The work also benefited from support of the Interdisciplinary Climate Investigation Center (INCLINE) research group at the University of São Paulo and NSF Award AGS-1303828 (to M.V.).

1. Bond G, et al. (1993) Correlation between climate records from North Atlantic sediments and Greenland ice. *Nature* 365:143–147.
2. Clement AC, Peterson LC (2008) Mechanisms of abrupt climate change of the last glacial period. *Rev Geophys* 46:RG4002.
3. Rasmussen SO, et al. (2014) Stratigraphic framework for abrupt climatic changes during the last glacial period based on three synchronized Greenland ice-core records: Refining and extending the INTIMATE event stratigraphy. *Quat Sci Rev* 106: 14–28.

4. WAIS Divide Project Members (2015) Precise interpolar phasing of abrupt climate change during the last ice age. *Nature* 520:661–665.
5. Andrews JT (1998) Abrupt changes (Heinrich events) in late Quaternary North Atlantic marine environments: A history and review of data and concepts. *J Quat Sci* 13:3–16.
6. Heinrich H (1988) Origin and consequences of cyclic ice rafting in the northeast Atlantic ocean during the past 130,000 years. *Quat Res* 29:142–152.
7. Hemming SR (2004) Heinrich events: Massive late Pleistocene detritus layers of the North Atlantic and their global climate imprint. *Rev Geophys* 42:RG1005.
8. Barker S, et al. (2009) Interhemispheric Atlantic seesaw response during the last deglaciation. *Nature* 457:1097–1102.
9. Sánchez-Goñi MF, Harrison SP (2010) Millennial-scale climate variability and vegetation changes during the last glacial: Concepts and terminology. *Quat Sci Rev* 29: 2823–2827.
10. Hurrel JW, Deser C (2009) North Atlantic climate variability: The role of the North Atlantic Oscillation. *J Mar Syst* 78:28–41.
11. Yoshimori M, Broccoli AJ (2008) Equilibrium response of an atmosphere–mixed layer ocean model to different radiative forcing agents: Global and zonal mean response. *J Clim* 21:4401–4423.
12. Cvijanovic I, Chiang JCH (2013) Global energy budget changes to high latitude North Atlantic cooling and the tropical ITCZ response. *Clim Dyn* 40:1435–1452.
13. Schneider T, Bischoff T, Haug GH (2014) Migrations and dynamics of the intertropical convergence zone. *Nature* 513:45–53.
14. Mulitza S, et al. (2017) Synchronous and proportional deglacial changes in Atlantic meridional overturning and northeast Brazilian precipitation. *Paleoceanogr* 32: 622–633.
15. Naughton F, et al. (2009) Wet to dry climatic trend in north-western Iberia within Heinrich events. *Earth Planet Sci Lett* 284:329–342.
16. Barker S, et al. (2015) Icebergs not the trigger for North Atlantic cold events. *Nature* 520:333–336.
17. Naughton F, et al. (2016) Climate variability across the last deglaciation in NW Iberia and its margin. *Quat Int* 414:9–22.
18. Voelker AHL, de Abreu L (2011) A review of abrupt climate change events in the Northeastern Atlantic Ocean (Iberian Margin): Latitudinal, longitudinal and vertical gradients. *Abrupt Climate Change: Mechanisms, Patterns, and Impacts*, eds Rashid H, Polyak L, Mosley-Thompson E (AGU, Washington, DC), pp 15–37.
19. Zhang W, et al. (2014) A detailed East Asian monsoon history surrounding the 'Mystery Interval' derived from three Chinese speleothem records. *Quat Res* 82: 154–163.
20. Arz HW, Pätzold J, Wefer G (1998) Correlated millennial-scale changes in surface hydrography and terrigenous sediment yield inferred from last-glacial marine deposits off Northeastern Brazil. *Quat Res* 50:157–166.
21. Dupont LEM, et al. (2010) Two-step vegetation response to enhanced precipitation in Northeast Brazil during Heinrich event 1. *Glob Change Biol* 16:1647–1660.
22. Jaeschke A, Rühlemann C, Arz H, Heil G, Lohmann G (2007) Coupling of millennial-scale changes in sea surface temperature and precipitation off northeastern Brazil with high-latitude climate shifts during the last glacial period. *Paleoceanogr* 22: PA4206.
23. Stríkis NM, et al. (2015) Timing and structure of Mega-SACZ events during Heinrich Stadial 1. *Geophys Res Lett* 45:1–8.
24. Rhodes RH, et al. (2015) Paleoclimate. Enhanced tropical methane production in response to iceberg discharge in the North Atlantic. *Science* 348:1016–1019.
25. Vuille M, Bradley RS, Werner M, Healy R, Keimig F (2003) Modeling $\delta^{18}O$ in precipitation over the tropical Americas: 1. Interannual variability and climatic controls. *J Geophys Res* 108:4174.
26. Vuille M, Werner M (2005) Stable isotopes in precipitation recording South American summer monsoon and ENSO variability: Observations and model results. *Clim Dyn* 25: 401–413.
27. Cheng H, et al. (2013) Climate change patterns in Amazonia and biodiversity. *Nat Commun* 4:1411.
28. Wang X, et al. (2004) Wet periods in northeastern Brazil over the past 210 kyr linked to distant climate anomalies. *Nature* 432:740–743.
29. Mosblech NAS, et al. (2012) North Atlantic forcing of Amazonian precipitation during the last ice age. *Nat Geosci* 5:817–820.
30. Kanner LC, Burns SJ, Cheng H, Edwards RL (2012) High-latitude forcing of the South American summer monsoon during the last glacial. *Science* 335:570–573.
31. Wang X, et al. (2017) Hydroclimate changes across the Amazon lowlands over the past 45,000 years. *Nature* 541:204–207.
32. Austin WEN, Hibbert FD (2012) Tracing time in the ocean: A brief review of chronological constraints (60-8 kyr) on North Atlantic marine event-based stratigraphies. *Quat Sci Rev* 36:28–37.
33. Stanford JD, et al. (2011) A new concept for the paleoceanographic evolution of Heinrich event 1 in the North Atlantic. *Quat Sci Rev* 30:1047–1066.
34. de Abreu L, Shackleton NJ, Schoenfeld J, Hall M, Chapman M (2003) Millennial-scale oceanic climate variability off the western Iberian margin during the last two glacial periods. *Mar Geol* 196:1–20.
35. Salgueiro E, et al. (2010) Temperature and productivity changes off the western Iberian margin during the last 150 ky. *Quat Sci Rev* 29:680–695.
36. Bard E, Rostek F, Turon JL, Gendreau S (2000) Hydrological impact of Heinrich events in the subtropical northeast Atlantic. *Science* 289:1321–1324.
37. Hodell DA, et al. (2017) Anatomy of Heinrich layer 1 and its role in the last deglaciation. *Paleoceanogr* 32:284–303.
38. Stern JV, Lisiecki LE (2013) North Atlantic circulation and reservoir age changes over the past 41,000 years. *Geophys Res Lett* 40:1–5.
39. Novello VF, et al. (2017) A high-resolution history of the South American monsoon from last glacial maximum to the Holocene. *Sci Rep* 7:44267.
40. Chiang JCH, Bitz CM (2005) Influence of high latitude ice cover on the marine intertropical convergence zone. *Clim Dyn* 25:477–496.
41. Deplazes G, et al. (2013) Links between tropical rainfall and North Atlantic climate during the last glacial period. *Nat Geosci* 6:213–217.
42. Wang YJ, et al. (2001) A high-resolution absolute-dated late Pleistocene monsoon record from Hulu Cave, China. *Science* 294:2345–2348.
43. Hoff U, Rasmussen TL, Stein R, Ezat MM, Fahl K (2016) Sea ice and millennial-scale climate variability in the Nordic seas 90 kyr ago to present. *Nat Commun* 7:12247.
44. Wassenburg JA, et al. (2016) Reorganization of the North Atlantic Oscillation during early Holocene deglaciation. *Nat Geosci* 9:602–605.
45. Cruz FW, et al. (2009) Orbitally driven east-west antiphasing of South American precipitation. *Nat Geosci* 2:1–5.
46. Broecker WS, Putnam AE (2013) Hydrologic impacts of past shifts of Earth's thermal equator offer insight into those to be produced by fossil fuel CO_2. *Proc Natl Acad Sci USA* 110:16710–16715.
47. Putnam AE, Broecker WS (2017) Human-induced changes in the distribution of rainfall. *Sci Adv* 3:e1600871.
48. Cheng H, et al. (2013) Improvements in ^{230}Th dating, ^{230}Th and ^{234}U half-life values, and U–Th isotopic measurements by multi-collector inductively coupled plasma mass spectrometry. *Earth Planet Sci Lett* 371:82–91.
49. Stuiver M, Grootes PM (2000) GISP2 oxygen isotope ratios. *Quat Res* 53:277–284.
50. Grootes PM, Stuiver M, White JWC, Johnsen S, Jouzel J (1993) Comparison of oxygen isotope records from the GISP2 and GRIP Greenland ice cores. *Nature* 366:552–554.
51. Seierstad IK, et al. (2014) Consistently dated records from the Greenland GRIP, GISP2 and NGRIP ice cores for the past 104 ka reveal regional millennial-scale $\delta^{18}O$ gradients with possible Heinrich event imprint. *Quat Sci Rev* 106:29–46.
52. Berger A, Loutre MF (1991) Insolation values for the climate of the last 10 million years. *Quat Sci Rev* 10:297–317.